Available online at www.sciencedirect.com
SCIENCE DIRECT®
Journal of Nuclear Materials 326 (2004) 201–210
journal of nuclear materials
www.elsevier.com/locate/jnucmat

# Corrosion/precipitation in non-isothermal and multi-modular LBE loop systems

Jinsuo Zhang *, Ning Li

*Los Alamos National Laboratory, Center for Non-linear Studies, CNLS, MS-B258, Los Alamos, NM 87545, USA*

Received 8 August 2003; accepted 13 January 2004

**Abstract**

Precise simulations of all hydrodynamic conditions encountered in practical lead–bismuth eutectic (LBE) coolant loop systems by use of flowing conditions in the laboratory are difficult and expensive, if not impossible. Therefore it is important and necessary to develop corrosion models to predict corrosion behaviors at the design stage of practical LBE coolant systems and to properly interpret and apply experimental results from test loops. In the present study, we extended a kinetic corrosion model for a simple LBE loop to a model for a loop with multiple modules to include effects of geometry variations. The model is applied to an ideal loop with contractions and expansions and a test loop named 'DELTA' set up in the Los Alamos National Laboratory. Analyses show the combined effects of the axial geometry variations and the axial temperature profile on the corrosion/precipitation distribution in the entire loop. The present study illustrates systematically different dependence of corrosion behaviors on the hydraulic factors in an open pipe flow, a simple loop flow and a multi-modular loop flow.


## 1. Introduction

Liquid metals have several possible applications in nuclear energy systems [1]. Lead and lead alloys, such as lead–bismuth eutectic (LBE), are efficient heat transfer media because of high thermal conductivity and high heat capacity. Moreover, LBE is chemically inert and does not react violently with air and water [2]. Therefore, LBE is one of coolant candidates in advanced reactors and accelerator driven systems (ADS) [2,3]. However, LBE is very corrosive to many structure materials if they are exposed to LBE directly. Corrosion in the form of dissolution, intergranular penetration, and interstitial transfer to and/or from the liquid metal can result in significant wall thinning and/or loss of mechanical integrity [1]. Hence, one of the critical obstacles to the wide use of LBE as a nuclear coolant is corrosion. Corrosion problems need to be controlled and mitigated, or they lead to severe safety problems [3,4].

A large number of closed loop systems have been set up to study the flow-affected corrosion mechanisms. They are simple and convenient, and representative geometry can be tested in a constant environment for a fixed period [5]. In LBE technology development programs, test loops are typically made of the same type of steel as the test materials. Therefore, the up-/downstream effects should be properly included in the analysis of the experimental data. Investigations on corrosion in LBE are being carried out in many programs [6–9]. The experimental results indicate that the flow-affected corrosion depends on many factors: time of exposure, temperature, thermal gradient, solid and liquid compositions, flow velocity, etc., and occurs through several mechanisms: mass transport, phase transport, erosion–corrosion and cavitation–corrosion [10]. The dependence of corrosion on local hydraulic factors has

* Corresponding author. Tel.: +1-505 667 7444; fax: +1-505 665 2659.
*E-mail address:* jzhang@cnls.lanl.gov (J. Zhang).

0022-3115/$ - see front matter © 2004 Elsevier B.V. All rights reserved.
doi:10.1016/j.jnucmat.2004.01.013

been amply studied through modeling of the local mass transfer coefficient, but there are few studies systematically investigated the global distribution effects, such as the axial temperature profile and axial geometry variation effects.

In a non-isothermal LBE loop system, corrosion occurs in the hot regions and the corrosion products are subsequently deposited in some cooler areas. The deposition may lead to severe flow path restriction that can eventually block the flow. Most of the test facilities are set up for corrosion tests and the data for deposition of corrosion products is much more scarce compared to the corrosion data.

Precise simulations of all hydrodynamic conditions encountered in practice by use of flowing conditions in the laboratory are difficult and expensive, if not impossible. However, it is important to understand the flow-affected corrosion mechanisms in order to control and mitigate corrosion in LBE systems. Therefore theoretical analyses are very important and necessary to provide general information on flow-affected corrosion. Several corrosion models have been developed in aqueous media based on experimental results [11–13]. Assuming the corrosion product bulk concentration to be zero, Balbaud-Celerier and Barbier [10] applied these models to calculate corrosion rates in liquid metal loops. They obtained much higher values than the experimental results. Therefore an accurate description of the corrosion phenomena that take place in a non-isothermal system can be accomplished only if the axial conditions are taken into consideration.

Assuming the corrosion product concentration equaling that in the cold zone, Epstein [14] developed a model that could predict the mean corrosion rate at the hot zone in heat transfer loops. Zhang and Li [15] improved the local corrosion models for closed loop systems by including the fact that the amount of corrosion should equal to the amount of deposition of corrosion products at steady state. The improved model still can only provide the mean corrosion rate in the hot region. Sannier and Santarini [16] developed a corrosion model that could predict the corrosion and deposition zones. Employing the model, the authors obtained good results consistent with the experimental results for a natural convection lead loop, indicating that the model has reasonable performance. However, the authors assumed that the mass transfer boundary layer was only a function of the liquid metal velocity and the thickness remained the same along the loop, which is not reasonable for a loop with large thermal gradients.

In recent studies, a kinetic model based on some reasonable assumptions [17,18] was developed to investigate the dependence of corrosion/precipitation on the axial temperature profile for simple closed LBE loops. The studies show that corrosion/precipitation rate and distribution in a closed LBE loop system depend on both the local temperature and the axial temperature profile, which cautions us that corrosion test results obtained from one flow loop cannot be directly applied to another loop with different axial temperature profile. However, the model is limited to simple loops with constant cross-section. Generally, geometry variations in the axial direction are unavoidable in engineering applications. Such variations lead to varying hydrodynamic conditions [19], which will alter the corrosion rate and distribution. The purpose of the present study is to determine the combined effects of the axial geometry variations and the axial temperature profile on the corrosion/precipitation distribution in non-isothermal LBE loops with multiple modules.

It has been recognized that corrosion behaviors of steels in LBE depend on the oxygen concentration in the liquid alloy. The active oxygen control technique [20] exploits the fact that lead and bismuth are chemically less active than the major components of steels, such as Fe, Ni, and Cr. By carefully controlling the oxygen concentration in LBE, it is possible to maintain an iron and chrome oxide based film on structural steels, while keeping lead and bismuth from excessive oxidization that can lead to lead oxide precipitation. The oxide film, especially the compact portion rich in Cr effectively separates the substrates from LBE. Once the oxide film is formed on the structure surface, the direct dissolution of the structural materials becomes negligible because the diffusion rates of the alloying components are very small in the protective oxide layer. Under such circumstance, the only effective mean of transferring structural materials into LBE is through the reduction of the oxide film at the interface of the film and LBE. At low oxygen concentration, the protective oxide layer cannot be formed and the corrosion is through direct dissolution of the materials to LBE. In the present study, both processes are considered.

We extend the simple corrosion model [17] to a model that can be applied to non-isothermal and multi-modular loops with or without oxygen control. The model is applied to a non-isothermal ideal loop with contractions and expansions and a material test loop (named as DELTA loop) built and operated in the Los Alamos National Laboratory. Distributions of the corrosion/precipitation rate are studied to determine the dependence of the corrosion/precipitation rate on the axial geometry variations and the axial temperature profile. The bulk concentration of the corrosion product varies along the axis and the variation is small enough to be neglected. The amount of highest corrosion/precipitation and the corrosion/precipitation areas can be determined. The model provides information on what we have to take into consideration when analyzing experimental results from a non-isothermal LBE test loop. The non-local analysis also illustrates means to control the corrosion/precipitation rate profile and to control the corrosion/

precipitation rate through designing geometry and controlling the axial temperature profile.

## 2. Theory

### 2.1. Corrosion model for non-isothermal simple loops

The authors adopted the following assumptions in developing a corrosion model for simple loops [17]: (1) The reaction term contributes little to the mass transfer in the bulk flow; (2) the flow is fully turbulent; (3) the fluid media is liquid metal and the mass diffusion coefficient is much less than the kinematic viscosity; (4) the physical properties of the flowing liquid and the bulk flow velocity stay constant along the loop axis; (5) the wall surface is smooth, the corrosion and precipitation do not change the wall surface enough to affect the fluid flow; (6) the mass transfer process is at a steady state. The convection–diffusion mass transfer equation in the mass transfer boundary layer is simplified to

$$\gamma y\frac{\partial c}{\partial x}=D\frac{\partial^2 c}{\partial y^2}, \tag{1}$$

where $c$ (wppm) is the corrosion product concentration, $x$ (m) and $y$ (m) are coordinates in the axial and transverse directions, respectively, $D$ ($m^2/s$) is the diffusion coefficient, $\gamma$ ($s^{-1}$) is the wall shear rate and it is constant along the loop here and can be calculated by $\gamma=\lambda V^2/2\upsilon$ ($\lambda$ is the Fanning friction factor, $V$ (m/s) is the bulk flow velocity outside the boundary layer and $\upsilon$ ($m^2/s$) is the kinematic viscosity). The corrosion/precipitation rate for a non-isothermal liquid metal closed loop is obtained [17]:

$$q(\xi)=-D\left.\frac{\partial c}{\partial y}\right|_{y=0}=\left(\frac{2\pi D^2\gamma}{3L}\right)^{1/3}\frac{1}{Ai(0)\Gamma(1/3)}\times\sum_{k\neq 0}Q_k\exp(2\pi k\mathrm{i}\xi), \tag{2}$$

where $L$ (m) is the loop length, $\xi=x/L$ is the non-dimensional coordinate in the axial direction, $Ai$ and $\Gamma$ are Airy function and Gamma function, respectively, and $Q_k=a_k k^{1/3}\mathrm{i}^{1/3}$ for $k>0$ and $Q_k=a_k|k|^{1/3}(-\mathrm{i})^{1/3}$ for $k<0$. i is the imaginary unit and $\mathrm{i}^{1/3}=\sqrt{3}/2+\mathrm{i}/2$ and $(-\mathrm{i})^{1/3}=\sqrt{3}/2-\mathrm{i}/2$ [17]. For a non-isothermal closed loop, the corrosion product surface concentration is a function of the axial coordinate and can be expressed as the following Fourier series:

$$c_{\mathrm{w}}(\xi)=\sum_k a_k\exp(2\pi\mathrm{i}k\xi). \tag{3}$$

Therefore, if the surface corrosion product concentration is given, the corrosion/precipitation rate and the profile can be obtained through Eq. (2) that is easily implemented in a computer program. Eq. (2) is limited to loops that have constant hydraulic diameters.

### 2.2. Corrosion model for non-isothermal and multi-modular loops

Geometry variations along the axis are unavoidable in engineering applications. Even for simple loops, the flow area can be changed through corrosion and deposition during long-term operations. Such geometry variations lead to varying hydrodynamic conditions, which will alter the corrosion distribution in such systems. For a flow loop with multiple modules, the wall shear rate is not constant along the axis and it varies with changing geometry. Neglecting the transition effects, we obtain from Eq. (1)

$$\bar{\gamma}F(x)y\frac{\partial c}{\partial x}=D\frac{\partial^2 c}{\partial y^2}, \tag{4}$$

where $\bar{\gamma}$ ($s^{-1}$) is the reference wall shear rate. $F(x)$ is the ratio of the local wall shear rate to the reference wall shear rate and it is not zero. Introducing

$$\zeta=\int_0^x\frac{1}{F(s)}\,\mathrm{d}s\quad\text{and}\quad\overline{L}=\int_0^L\frac{1}{F(s)}\,\mathrm{d}s.$$

Eq. (4) becomes to

$$\bar{\gamma}y\frac{\partial c}{\partial\zeta}=D\frac{\partial^2 c}{\partial y^2}, \tag{5}$$

that has the same form with Eq. (1). Therefore, the solution of the corrosion flux $q$ as a function of $\xi$ ($\xi=\zeta/\overline{L}$) can be expressed as:

$$q(\xi)=a+\left(\frac{2\pi D^2\bar{\gamma}}{3\overline{L}}\right)^{1/3}\frac{1}{Ai(0)\Gamma(1/3)}\sum_{k\neq 0}Q_k\exp(2\pi k\mathrm{i}\xi), \tag{6}$$

where $a$ is a constant. Because the total amount of corrosion equals the total amount of precipitation over the entire loop for a closed system at a steady state, then $a$ can be determined through the following integration:

$$\int_0^L\pi d(x)q(x)\,\mathrm{d}x=0, \tag{7}$$

where $d(x)$ is the local hydraulic diameter.

Finally, to complete the development of the analytical solution, the value of $F(x)$ needs to be specified. It can be obtained from some experimental data, analytical solutions or numerical simulations. In the present study, the transition effects are neglected, then $F(x)$ is determined by $d(x)$. Since the flow rate through each cross-section is constant for a closed loop, we get:

$$F(x)=\frac{\gamma(x)}{\bar{\gamma}}=\frac{\lambda(x)d(x)^{-4}}{\bar{\lambda}\bar{d}^{-4}}=\left(\frac{d(x)}{\bar{d}}\right)^{-3.8}, \tag{8}$$

where the variables with a bar represent the reference values. The Blasius equation for the friction factor is employed ($\lambda=0.046Re^{-0.20}$ and $Re=Vd/\upsilon$).

### 2.3. Modeling corrosion product transport in the bulk flow

In the bulk flow, the transport process of the corrosion product in the flowing liquid metal satisfies the following mass balance equation:

$$\frac{\mathrm{d}[c_{\mathrm{b}}A(x)V(x)]}{\mathrm{d}x}=p(x)q[\xi(x)], \tag{9}$$

where $A$ ($\mathrm{m}^2$) is the flow area and $p$ (m) is the circumference. For circular pipe, $A=\pi d^2/4$ and $p=\pi d$ (the boundary layer thickness is neglected since it is much smaller than the hydraulic diameter), $c_{\mathrm{b}}$ (wppm) is the corrosion product bulk concentration. For simple loop systems, $A$, $p$ and $V$ are constant along the axis, then the solution of $c_{\mathrm{b}}$ for simple loop is:

$$c_{\mathrm{b}}(\xi)=c_{\mathrm{b}}^0+\frac{4}{Vd}\frac{(2\pi L^2D^2\gamma)^{1/3}}{3^{1/3}Ai(0)\Gamma(1/3)}\left\{\sum_{k>0}\frac{Q_k}{2\pi k\mathrm{i}}\exp(2\pi k\mathrm{i}\xi)+\sum_{k<0}\frac{Q_k}{-2\pi|k|\mathrm{i}}\exp(2\pi k\mathrm{i}\xi)\right\}, \tag{10}$$

where $c_{\mathrm{b}}^0$ is the average bulk concentration and equals the average surface concentration $a_0$ at the steady state. For multi-modular loop systems, $A$, $p$ and $V$ are functions of the axial coordinate $x$, while the volume flow rate $Q=A(x)V(x)$ is constant over the entire loop. The bulk concentration can be calculated using the following integration:

$$c_{\mathrm{b}}(\xi)=\frac{\bar{L}}{Q}\int_{\xi_0}^{\xi}F[x(s)]p[x(s)]q(s)\,\mathrm{d}s+c_{\mathrm{b}}(\xi_0), \tag{11}$$

where $c_{\mathrm{b}}(\xi_0)$ is the bulk concentration at $\xi=\xi_0$ and can be calculated by considering that the average bulk concentration equals the average surface concentration.

### 2.4. Modeling the surface corrosion product concentration in oxygen controlled LBE system

Corrosion of steels in LBE occurs via dissolution at very low oxygen concentrations, and through surface oxidation and reduction of surface oxides at higher oxygen concentrations. In either case, it is usually sufficiently fast and the corrosion process is limited by the mass transfer process. Therefore the corrosion products' concentrations are always at their saturated or equilibrium levels at the solid-liquid interface. For the dissolution process, the surface concentrations equal their saturated concentration [20]:

$$\log(c)=\log(c_{\mathrm{s}})=A_1+\frac{B_1}{T}, \tag{12}$$

where $T$ is the absolute temperature in Kelvin and $c$ is the concentration in wppm. The values of parameters $A_1$ and $B_1$ vary for species and some of them for common components in steels and oxygen can be found in Ref. [20].

In the reduction process, the protective $\mathrm{MO}_\beta$-based film can be reduced by Pb via the following reaction:

$$\frac{1}{\beta}\mathrm{MO}_\beta+\mathrm{Pb}=\frac{1}{\beta}\mathrm{M}+\mathrm{PbO}.$$

The equilibrium concentration of M is:

$$\log(c_{\mathrm{eq}})=A_2-\frac{B_2}{T}-\beta\log(c_{\mathrm{O}}), \tag{13}$$

where $c_{\mathrm{O}}$ is the oxygen concentration in LBE, $A_2$ and $B_2$ vary for species and can be calculated through analyzing the oxygen thermodynamic activity in LBE [20], for example, for iron [20], $A_2=11.35$, $B_2=12844$ and $\beta=4/3$.

There is a critical oxygen level in LBE, below which continuous iron oxide based protective film cannot form and the Fe concentration at the surface is calculated by Eq. (12), and above which the continuous iron oxide film can form and the Fe concentration is calculated by Eq. (13). It is not clear how these two regions connect to each other, Ref. [18] assumed that the species concentration at the surfaces is given by the minimum of the saturation concentration and the chemical equilibrium concentration. That is,

$$c_{\mathrm{w}}=\min(c_{\mathrm{s}},c_{\mathrm{eq}}). \tag{14}$$

The boundary between the dissolution regime and the reduction regime for iron (the main corrosion product)

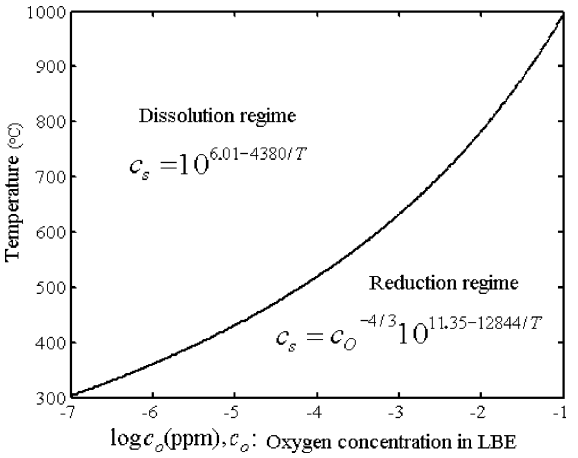


Fig. 1. The boundary between the dissolution and oxide reduction regimes as a function of temperature and oxygen concentration in LBE.

as a function of temperature and oxygen concentration is shown in Fig. 1. The figure shows that a higher oxygen level is needed to form continuous surface oxides at higher temperatures.

## 3. Analysis results and discussion

### 3.1. Comparison of theoretical and experimental results

Experimental results of corrosion tests performed in a non-isothermal simple lead loop are available [16]. The authors found that the corrosion depth for 10 CD 9–10 steel is between 75 and 110 μm after 3000 h and for Z 10 CD Nb V 92 steel is between 25 and 40 μm after 2800 h. In our previous paper [17], we calculated the corrosion rate at the test section of the liquid lead loop using the corrosion model for simple loop. The model predicts an iron corrosion depth between 40 and 70 μm per 3000 h, which agrees well with the experimental results. The deviations are not unexpected given the experimental uncertainties and alloy composition effects.

No experimental result on corrosion rate is available for LBE loops with oxygen control. A LBE loop called JLBL-1 loop (Fig. 2), was set up in the Japan Atomic Energy Research Institute and some initial experiments have been carried out to study the corrosion and deposition without actively controlling oxygen [21]. Fig. 2 shows a schematic depiction of the loop. All materials are 316 steel. The inner diameter of the circulating tube, the test tube at the low temperature and test tube at high temperature is 22, 22 and 10 mm, respectively. The flow velocity is 1 m/s at the high temperature test leg and 0.2 m/s in elsewhere. The oxygen concentration is not measured during the experiment. The corrosion rate is less than 0.1 mm per 3000 h [21] at the high temperature test leg. The deposition zones are shown in Fig. 2(a) in thick black line.

Since there is no oxide layer reported [22], it is assumed that the corrosion process is due to dissolution. To estimate corrosion/precipitation rate in the JLBL-1, the kinematic viscosity $\upsilon$ of LBE and the corrosion product diffusion coefficient $D$ of the iron in LBE are chosen as $\upsilon = 1.5 \times 10^{-7}$ m$^2$/s estimated from Davis and Shieh [23] and $D_{\mathrm{Fe}\rightarrow\mathrm{Pb\text{–}Bi}} = 10^{-9}$ m$^2$/s estimated from Ref. [18]. The calculated iron corrosion/precipitation rate profile and the temperature profile for JLBL-1 are shown in Fig. 3. The origin point is set at the beginning of the low temperature test leg. Fig. 3 shows that the deposition zones in JLBL-1 loop can be predicted exactly using the present non-isothermal and multi-modular corrosion model. The predicted corrosion rate in the hot test section is about 0.025 mm per 3000 h close to the experimental value of 0.03–0.1 mm [21]. Considering there are many uncertain factors: value of the diffusion coefficient and the surface concentration, effects of the materials composition, erosion, etc., the calculated values are consistent with the experiment results.

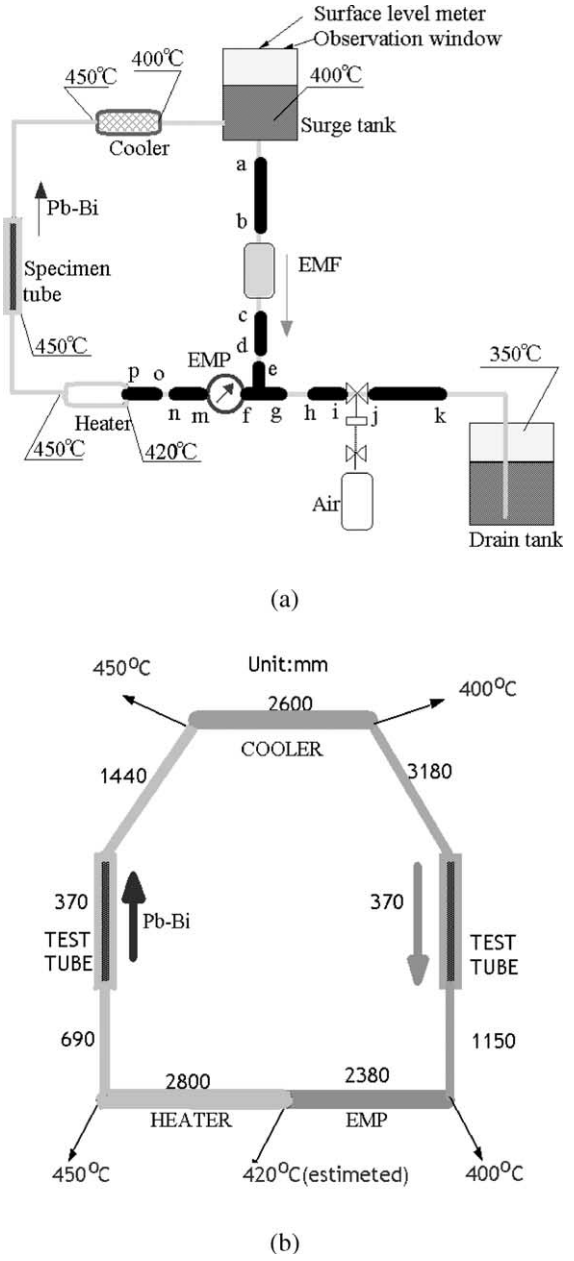


Fig. 2. Schematic drawing and parameters of JLBL-1 LBE loop. Experimentally observed precipitation zones are shown in (a) using thick black line.

### 3.2. Apply the model to a loop with sinusoidal surface concentration

Suppose that the species surface concentration has the following profile:

$c_w = \bar{c} + c_O \cos(2\pi x/L)$.

For a simple loop [$F(x) = 1$] with such surface concentration, He et al. [18] found that the corrosion/precipitation rate also varies sinusoidally along the loop, while, the highest corrosion/precipitation rate does not occur at the highest/lowest concentration. There is a phase shift between the highest corrosion/precipitation rate and the highest/lowest wall concentration. This phenomenon is due to the effects of axial temperature profile and the resultant axial wall concentration profile because there is no geometry variation in a simple loop.

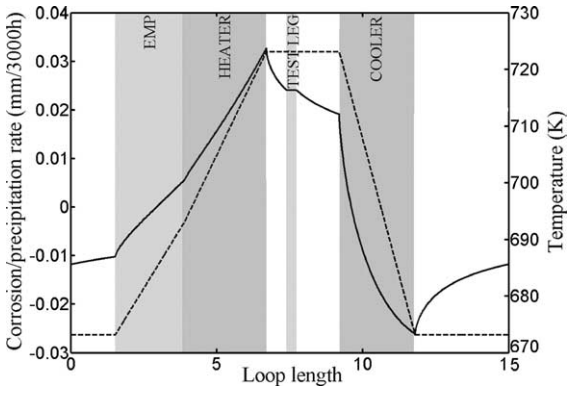


Fig. 3. Calculated corrosion/precipitation rate for iron (solid line) and the temperature profile (dashed line) for JLBL-1 loop. Positive value corresponds to corrosion and negative value corresponds precipitation.

For a loop with geometry variations along the axis, such as expansions and contractions, the corrosion/precipitation profile is influenced by the combined effects of the global temperature profile and the resultant surface corrosion product concentration profile, and the geometrical variations and the resultant wall shear rate profile. Fig. 4 shows some results obtained from the present model for multi-modular loops with sinusoidal surface concentration for four shear rate distributions. For comparison, the corrosion/precipitation curve for the simple loop with the same surface concentration is also shown in all the figures [Fig. 4(a)–(d)]. The figures indicate that an expansion or a contraction affects not only the local corrosion/precipitation rate but also the axial corrosion/precipitation distribution. The highest corrosion/precipitation rate can be reduced and its

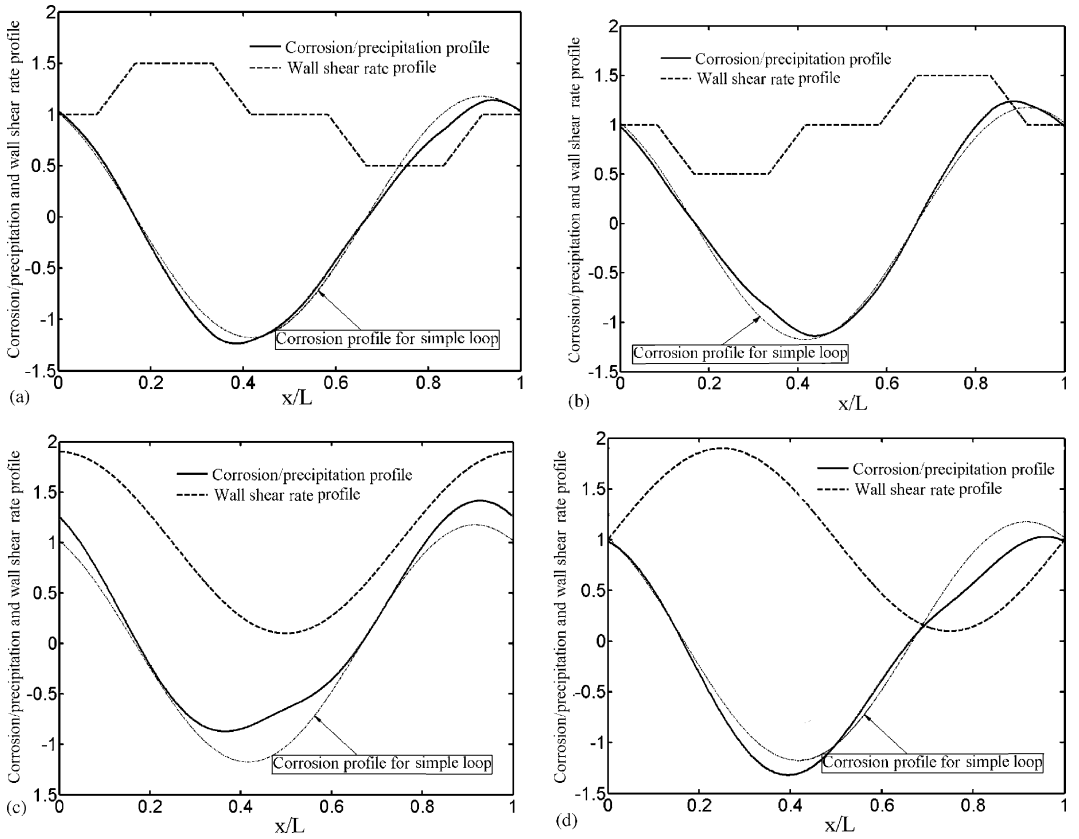


Fig. 4. Corrosion/precipitation rate for a sinusoidal surface concentration profile. The dashed line is for the simple loop with a constant cross-section. The flux is scaled as $q/\beta\bar{c}$ where $\beta = (2\pi D^2\gamma/3L)^{1/3}/Ai(0)\Gamma(1/3)$ and $\bar{c}/c_O = 0.9$.

location shifts to up- or down-stream through changing the cross-section at some locations along the loop.

The location of corrosion and precipitation zones depend on both the geometrical variations and the temperature profile of the loop system. The highest corrosion does not necessarily occur at the highest wall shear rate where the flow area is smallest and the bulk velocity reaches its highest value, even though the highest velocity may be at the location where the species reaches the highest surface concentration. Generally, increasing the local wall shear rate results in a larger local corrosion or precipitation rate. At the precipitation locations, the species precipitation decreases the flow area, leading to a higher wall shear rate and consequently higher precipitation rate. This positive feedback becomes stronger in time and may lead to flow blockage. Therefore, precipitation of corrosion products is an important consideration in assessing the use of any non-isothermal loop systems that are subject to corrosion.

The above analyses show that the corrosion/precipitation rate depends strongly on the global geometry and the temperature profile. Variations of the flow path in some sections can result in variations of corrosion/precipitation rate in other sections. For practical systems, the highest corrosion/precipitation rate should be reduced or the locations should be shifted to sections that can be easily replaced. The present analysis provides guidance on how to mitigate the highest corrosion/precipitation rate and shift their locations along the system through designing the geometry and controlling the temperature profile.

### 3.3. Applying the model to estimate the corrosion rate of the samples in DELTA loop

The above model is applied to DELTA loop set up in the Los Alamos National Laboratory. The DELTA loop is a non-isothermal closed loop and is used to study the corrosion of various materials in flowing LBE. Detailed description about the loop can be found in Refs. [18,24]. The loop is about 30 m long and the diameter of the circulating tube is 0.0525 m. The circulating tube is constructed by SS316. In the present calculations, we use $\upsilon = 1.5 \times 10^{-7}$ m$^2$/s and $D_{\mathrm{Fe}\rightarrow\mathrm{Pb\text{–}Bi}} = 10^{-9}$ m$^2$/s estimated from Ref. [18]. The corrosion/precipitation profile of the loop without the installed samples (simple loop) has been examined using the corrosion model for simple loops [17,18]. The results illustrate effects of the highest temperature, the temperature gradient, the oxygen concentration in LBE and the flow velocity on the local corrosion/precipitation rate and axial corrosion/precipitation profile.

When samples are installed in the highest temperature leg, the samples' holders change the flow area and the present multi-modular corrosion model is needed to predict the corrosion rate. The calculated corrosion/precipitation rates in the loop are shown in Fig. 5 for different hydraulic diameters $d_t$ at the test leg for the case with oxygen concentration $c_O = 0.01$ ppm and flow rate $Q = 0.0011$ m$^3$/s. The average corrosion rate at the test leg increases with the decreasing diameter. For this loop the flow area variation at the test leg has little influence over the corrosion/precipitation rates in other sections. The highest corrosion rate increases, while the highest precipitation rate decreases with the decreasing pipe diameter at the test leg. The locations of the highest corrosion and precipitation do not change.

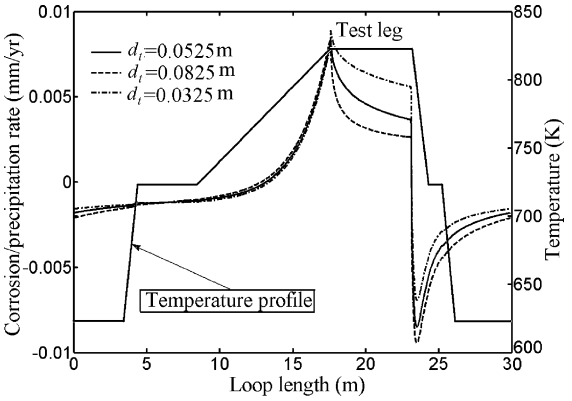


Fig. 5. Corrosion/precipitation rates of iron in DELTA loop for different pipe inner diameters at the test leg ($d_t$). $Q = 0.0011$ m$^3$/s and $c_O = 0.01$ ppm.

For a closed loop system subjected to corrosion, the bulk concentration of corrosion product increases with time until it reaches the steady state. The transient process can be very short if the test loop is constructed of materials with corrosion resistance similar to the test materials, as is the case for most LBE test loops. The calculated bulk concentration of iron (main corrosion product) in DELTA loop using the present model is shown in Fig. 6 (using the same parameters to those in Fig. 5). Clearly, the bulk concentration is not zero. Therefore, using the local corrosion model to predict the corrosion rate in an isothermal leg in a non-isothermal loop system results in a higher corrosion rate through assuming a zero bulk concentration. The bulk concentration varies around its average value that equals the surface average concentration and reaches its highest value at the end of the test leg, but the variation is small enough to be neglected and the bulk concentration can be assumed to be constant over the entire loop. Fig. 6 also shows that the average bulk concentration increases with the diameter at the test leg. This is because a larger diameter at the test leg results in a larger contact area between the liquid and the materials. A larger bulk concentration leads to a smaller corrosion rate.

In the mass transfer controlled regime, the corrosion rate can also be expressed in a dimensionless form

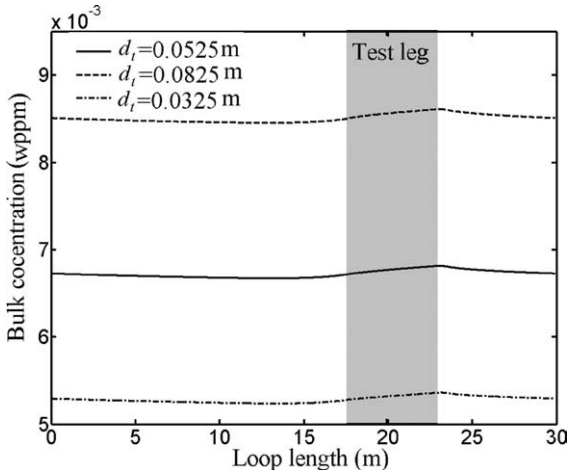


Fig. 6. Bulk concentrations of iron in DELTA loop for different tube pipe diameters at test leg. The parameters are the same as those in Fig. 5.

through the Sherwood number. At the test leg, the Sherwood number is defined by

$$Sh = \frac{Kd_t}{D}, \tag{15}$$

where $K$ (m/s) is the mass transfer coefficient and is calculated by

$$K = \frac{q}{c_w - c_b}. \tag{16}$$

Previous theoretical studies show that the mass transfer coefficient is proportional to $d^{-0.14}$ for open pipe flow [6] and $d^{-0.067}$ for simple close loop flow [18]. Both correlations show that increasing the hydraulic diameter leads to a smaller mass transfer coefficient. These relations are not exact for closed loops with multi-modular sections. The mass transport variations at the test leg expressed by the dimensional mass transfer coefficient and the dimensionless Sherwood number for different test leg diameters $d_t$ are shown in Fig. 7(a) and (b). For all the cases considered, the mass transfer coefficient and the Sherwood number decrease sharply at the beginning of the test leg and slowly downstream. Different from the cases of an open pipe flow and a simple closed loop flow, the local mass transfer coefficient increases with the increasing diameter at the test leg for the present case, which shows that the dependence of corrosion rate on the test leg diameter in multi-modular loops is system specific. Therefore, the experimental and theoretical relations for an open pipe flow or a simple loop flow cannot be applied directly to a loop with geometry variations along the axis. This cautions us that we need to consider the operating conditions when using experimental results from the same loop to scale the corrosion rate.

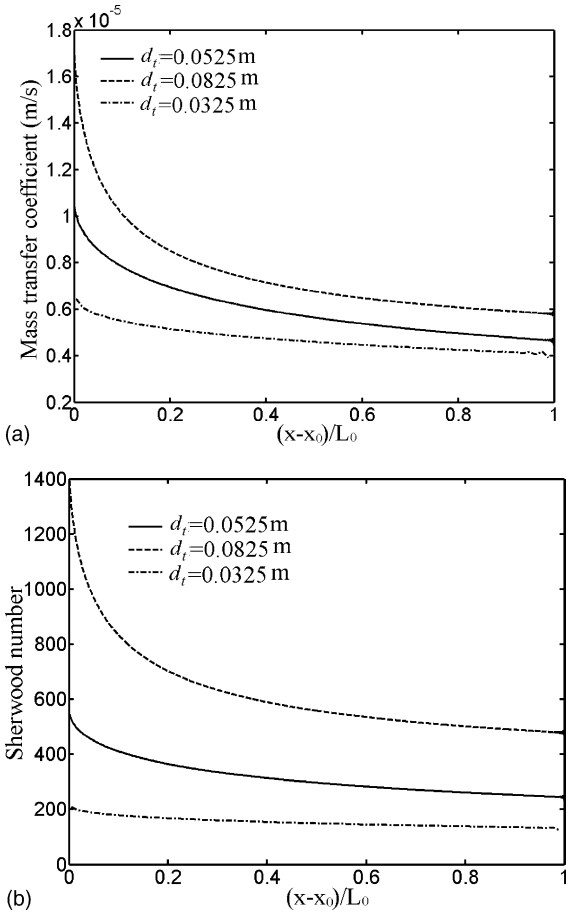


Fig. 7. Corrosion rate variations expressed by dimensional mass transfer coefficient $K$ (m/s) and non-dimensional Sherwood number at the test leg for different test leg diameters. Parameters are the same to those in Fig. 5. $x_0$: the beginning coordinate of the test leg, and $L_0$: the test leg length. (a) Mass transfer coefficient variations at the test leg of DELTA loop. (b) Sherwood number variations at the test leg of DELTA loop.

To illustrate the different dependencies of corrosion/precipitation on the hydraulic factors between the simple and the multi-modular loop systems, the calculated average corrosion rates at the test leg of the loop with the same temperature profile of DELTA loop are shown in Fig. 8 for two cases (constant velocity and constant flow rate in the test leg) for both simple loop (the diameter elsewhere is the same to the diameter at the test leg) and multi-modular loop (for different diameters at the test leg, the diameter elsewhere is kept at 0.0525 m). For the simple loop, the average corrosion rate is linear in $V^{0.60}d^{-0.067}$, indicating that the corrosion rate is proportional to $V^{0.60}d^{-0.067}$ and is consistent with the theoretical results [17]. For a constant velocity in the test leg, expansion results in a higher average corrosion rate while contraction results in a lower average corrosion

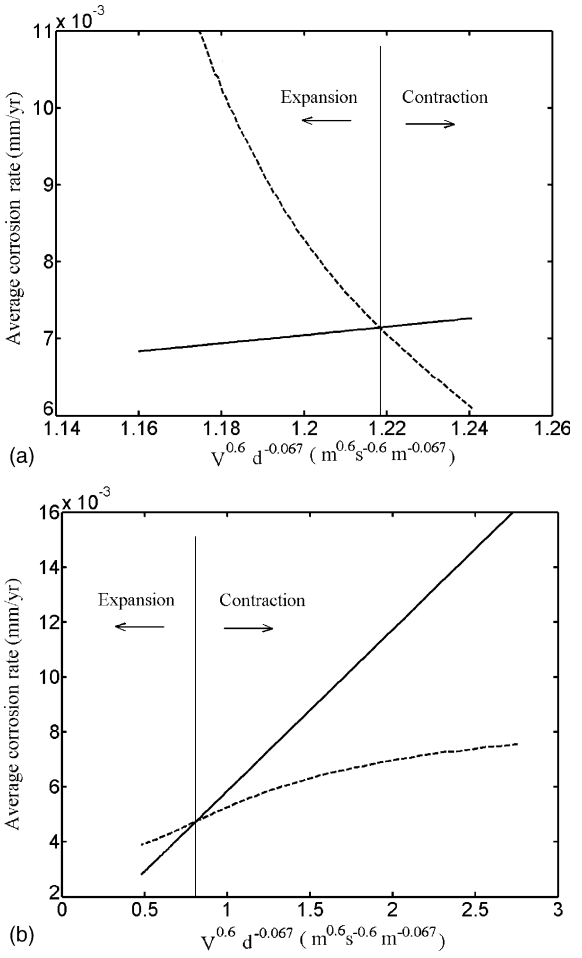


Fig. 8. Comparison of the average corrosion rate at the test leg versus diameter in a simple loop (solid line) and a multi-modular loop (dashed line). For simple loop, the diameters at other legs are the same to that at the test leg. For multi-modular loops, the diameters at other legs are kept 0.0525 m. All other parameters are the same to those in Fig. 5. (a) The velocity at the test leg has a constant value 1 m/s. (b) The flow rate at the test leg has a constant value 0.0011 $m^3/s$.

rate. For a constant flow rate, expansion and contraction have the opposite effects on the average corrosion rate compared to the constant velocity case. Even when all the parameters (velocity, hydraulic diameter and temperature) are the same in the test leg, corrosion rates for simple loops can be significantly different from those for loops with geometry variations. This shows that applying the local corrosion models to a constant temperature leg in a complex loop system may produce wrong corrosion rates.

The above calculations give a preliminary quantitative evaluation of the corrosion and deposition behaviors of materials in LBE systems. Up till now, there has been little information on the corrosion/deposition of steels in non-isothermal LBE systems. Some important factors remain uncertain. A complete experimental investigation on corrosion will be carried out in the DELTA loop at the Los Alamos National Laboratory. We plan to benchmark the key results obtained from the present theoretical model.

## 4. Summaries

Geometry changes along flow axis of liquid metal coolant loop systems are unavoidable in applications. In addition, corrosion and deposition of the containment materials themselves also change the flow area and affect the corrosion/deposition process. To fully understand the corrosion processes in non-isothermal coolant loop systems, geometry variations must be carefully considered. In the present study, we extend the kinetic corrosion model for simple loops, so that it can be applied to calculate the corrosion/precipitation rate in non-isothermal and multi-modular liquid metal loops. Several cases are studied to examine the combined effects of geometry variation and temperature profile. The model makes it possible to study the feedback effects of corrosion and precipitation themselves.

To benchmark the mathematic model, we compare the theoretical results with the experimental results from the JLBL-1 LBE loop. The model gives good predictions on the locations of corrosion product deposition zones and the average corrosion rate in the test section.

The model is applied to an ideal loop with sinusoidal surface concentration profile and a materials test loop in the Los Alamos National Laboratory to illustrate the combined effects of the axial conditions. It is found that:

(1) The local corrosion/precipitation rate and the axial corrosion/precipitation profile depend on both the axial geometry variations and the axial temperature profile. The effects of both are not independent of each other.
(2) The local corrosion/precipitation rate increases with the increasing local wall shear rate. Depositions reduce the local flow cross-section which results in a higher local wall shear rate. The feedback of deposition is positive and will lead to flow blockage, while the feedback of corrosion is negative.
(3) Increasing or decreasing the flow area at a section may affect corrosion elsewhere. The highest corrosion/precipitation does not necessarily occur at the location where the velocity reaches its highest/lowest value, neither does it necessarily occur at the highest/lowest temperature. The locations of the highest corrosion and precipitation can be shifted through changing the hydraulic diameter at some sections and the axial temperature profile.
(4) The local corrosion model, only considering the local condition effects, may predict incorrect corrosion

rate in the constant temperature leg in a non-isothermal and multi-modular loop system. One has to consider the global operating conditions when analyzing experimental results from test loops.

(5) The dependencies of corrosion/precipitation on hydraulic factors for a simple loop and a loop with multiple modules may be significantly different. For the DELTA loop, decreasing the pipe diameter at the test leg results in a higher local corrosion rate and a smaller mass transfer coefficient at the steady state.

(6) The local mass transfer coefficient at the highest temperature leg decreases sharply at the beginning of the test leg and slowly downstream.

(7) The corrosion product bulk concentration is not zero for closed loop systems and varies along the loop axis. But the variation is small enough to be neglected and the bulk concentration can be assumed to be constant. For the DELTA loop, decreasing the pipe diameter at the test leg results in a smaller mean corrosion product bulk concentration.

Finally, the present model assumes a mass transfer controlled corrosion process and neglects the transition effects. For high velocities, the surface reactions could control the corrosion processes. Other mechanisms such as erosion–corrosion or cavitation–corrosion need to be considered. In a practical LBE coolant system, there are many complex structures, such as elbows, multi-branches, gauges etc. Such geometry variations along the axis may result in a highly intense vortex flow structures and lead to a high local corrosion/precipitation rate. These effects will be considered in future studies. Another aspect to be incorporated is the oxide growth at the LBE/steel interface, which plays an important roles as the protection barriers in oxygen controlled LBE system, through which corrosion and precipitation take place.

## Acknowledgements

This research is supported by Department of Energy under contact number W-7405-ENG-36.

## References

[1] P.F. Tortorelli, O.K. Chopra, J. Nucl. Mater. 104 (1981) 621.
[2] B.F. Gromov, Y.S. Belomitcev, et al., Nucl. Eng. Des. 173 (1997) 207.
[3] J.J. Park, D.P. Butt, C.A. Beard, Nucl. Eng. Des. 196 (2000) 315.
[4] J. Konys, H. Muscher, Z. Voss, O. Wedemeyer, J. Nucl. Mater. 296 (2001) 289.
[5] Z. Ahmed, B.J. Abdul Aleem, J. Mater. Eng. Perform. 3 (1994) 393.
[6] F. Barbier, A. Rusanov, J. Nucl. Mater. 296 (2001) 231.
[7] G. Muller, A. Heinzel, et al., J. Nucl. Mater. 301 (2002) 40.
[8] P. Deloffre, A. Terlain, F. Barbier, J. Nucl. Mater. 301 (2002) 35.
[9] G. Benamati, C. Fazio, H. Piankova, A. Rusanov, J. Nucl. Mater. 301 (2002) 23.
[10] F. Balbaud-Celerier, F. Barbier, J. Nucl. Mater. 289 (2001) 227.
[11] F.P. Berger, K.F.F.L. Hau, Int. J. Heat Mass Transfer 20 (1977) 1185.
[12] D.C. Silverman, Corrosion 40 (1984) 220.
[13] P. Harriott, R.M. Hamilton, Chem. Eng. Sci. 20 (1965) 1073.
[14] L.F. Epstein, Liquid Metals Technol. 20 (1957) 67.
[15] J. Zhang, N. Li, Nucl. Technol. 144 (3) (2003) 379.
[16] J. Sannier, G. Santarini, J. Nucl. Mater. 107 (1982) 196.
[17] J. Zhang, N. Li, J. Nucl. Mater. 321 (2003) 184.
[18] X. He, N. Li, M. Mineev, J. Nucl. Mater. 297 (2001) 214.
[19] T.Y. Rizk, G.E. Thompson, J.L. Dawson, Corros. Sci. 38 (1996) 1801.
[20] N. Li, J. Nucl. Mater. 300 (2002) 73.
[21] K. Kikuchi, private communications.
[22] K. Kikuchi, Y. Kurata, S. Saito, M. Futakawa, T. Sasa, H. Oigawa, E. Wakai, K. Miura, J. Nucl. Mater. 318 (2003) 348.
[23] C.B. Davis, A.S. Shieh, in: Proceedings of ICONE-8, 2–6 April, 2000.
[24] V. Tcharnotskaia, C. Ammerman, T. Daring, J. King, N, Li, D. Shaw, L. Snodgrass, K. Woloshun, in: Proceeding of ADTTA/AccApp'01, 2001.